Journal of chemical & engineering data

Article

Cite This: J. Chem. Eng. Data 2019, 64, 4349−4356

pubs.acs.org/jced

Solubility, Solubility Modeling, and Antisolvent Precipitation of 1,3-Bis(9-carbazolyl)benzene in Organic Solvents

Yuanzuo Zou,[†] Hong Huang,[‡] Yuan Pu,[†] Jie-Xin Wang,[†] Dan Wang,*[,†] and Jian-Feng Chen[†]

[†]State Key Laboratory of Organic-Inorganic Composites, Beijing University of Chemical Technology, Beijing 100029, China

[‡]Guangzhou China Ray Optoelectronic Materials Co., Ltd, Guangzhou, Guangdong 510663, China

ABSTRACT: The solubility of 1,3-bis(9-carbazolyl)benzene (mCP) in 12 kinds of organic solvents, including methanol, ethanol, isopropanol, *n*-butanol, ethyl acetate, *n*-hexane, dichloromethane, toluene, acetonitrile, tetrahydrofuran, 1-methyl-2-pyrrolidinone, and dimethyl sulfoxide was measured at 283.15−313.15 K and atmospheric pressure by using the isothermal saturation method. The experimental data in all solvents were correlated by the modified Apelblat equation. The results showed that the increase of temperature would lead to an increase of mCP solubility, and the correlated values based on the modified Apelblat equation agreed well with the experimental values. The maximum value of the root-mean-square deviation was 3.44×10^{-3}. Moreover, 1-methyl-2-pyrrolidinone with high solubility from the measuring data was used as a solvent to carry out solvent−antisolvent precipitation experiments in both conversional stirred-tank reactor and rotating packed bed. Under different experimental conditions, the size distribution of precipitation products varied greatly from 33 nm to 3.2 μm and the features of the shape varied from clavate crystals and stacked ellipsoids.

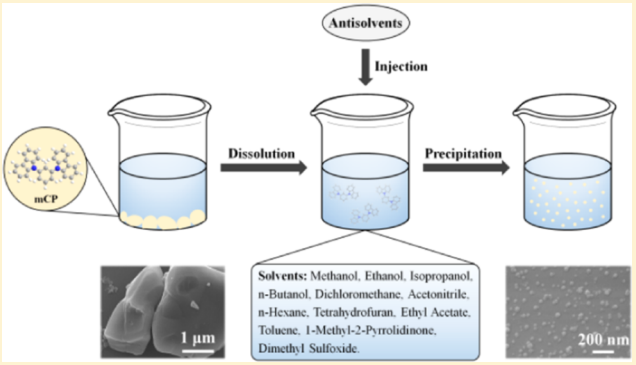

1. INTRODUCTION

Organic light-emitting diodes (OLEDs) are now widely used in the fields of display and illumination and are rapidly developing in the direction of flexibility, low cost, industrialization, and controllable size.[1−5] For the mainstream demand, solution-processed technology is being paid attention to, such as screen printing,[6] inkjet printing,[7,8] spin coating,[9] and contact printing.[10] The solubility of the OLED functional layer materials in organic solvents is an important parameter of the solution-processed technology.[11−19] Most of the conversional OLED materials are poorly soluble in organic solvents, which are difficult to be formulated as inks for printing. According to the previous research in nanoscience and nanotechnology, the organic particles with reduced size in nanoscale usually exhibit unique thermodynamic and kinetic characteristics that the bulk materials display.[20−23] In particular, the solubility of organic particles can be enhanced when the particle size decreased on the basis of the Ostwald−Freundlich equation.[20] Therefore, the nanonization of poorly soluble organic materials offers a promising approach for inks of OLED materials. The solvent−antisolvent (SAS) method has been the most straightforward technique to produce nanoparticles, and the solubility data of the organic solid solute in various solvents is fundamental to develop SAS processing for organic nanoparticles.[24−26] Carbazole and its derivatives have been widely studied at home and abroad and are used in the field of organic materials for optoelectronics, due to their strong hole-transport ability and high triplet energy.[27,28] The small molecular material 1,3-bis(9-carbazolyl)benzene (mCP) with simple molecular structure (Figure 1) and triplet energy up to 2.9 eV has been a hot research object for vacuum deposition of phosphorescent OLEDs.[29−31] However, the solubility data of mCP in various solvents are rarely reported.

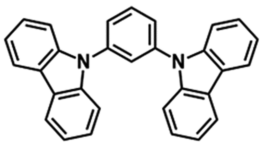

Figure 1. Chemical structure of 1,3-bis(9-carbazolyl)benzene (mCP).

In this work, we reported the solubility data of mCP in 12 organic solvents, including methanol, ethanol, isopropanol, *n*-butanol, ethyl acetate, *n*-hexane, dichloromethane, toluene, acetonitrile, tetrahydrofuran (THF), 1-methyl-2-pyrrolidinone (NMP), and dimethyl sulfoxide (DMSO), which were measured by the isothermal saturation method at atmospheric pressure. The organic solvents are selected from common liquid solvents, including alkanes and alcohols with various long chains, as well as halogenated solvents and aromatic solvents. Except for dichloromethane and DMSO, due to the special melting and boiling points, the measured temperature mainly ranged from

Received: May 15, 2019
Accepted: August 28, 2019
Published: September 9, 2019

DOI: 10.1021/acs.jced.9b00432
J. Chem. Eng. Data 2019, 64, 4349−4356

Table 1. Detailed Information on the Materials Used in the Work

chemicals	CAS registry number	molar mass (g mol^{-1})	density[a] (kg m^{-3})	source	mass fraction purity
mCP	550378-78-4	408.49		Sigma-Aldrich	0.970
NPB[b]	123847-85-8	588.74		Sigma-Aldrich	0.990
THF	109-99-9	72.11	890	Aladdin-Shanghai	0.990
ethanol	64-17-5	46.07	789	Aladdin-Shanghai	0.997
NMP	872-50-4	99.13	1028	Aladdin-Shanghai	0.995
n-hexane	110-54-3	86.18	660	Aladdin-Shanghai	0.990
DMSO	67-68-5	78.13	1100	Aladdin-Shanghai	0.995
ethyl acetate	141-78-6	88.11	902.3	Macklin-Shanghai	0.995
n-butanol	71-36-3	74.12	809.8	Macklin-Shanghai	0.990
toluene	108-88-3	92.14	863.6	Macklin-Shanghai	0.995
methanol	67-56-1	32.04	791.8	Macklin-Shanghai	0.995
dichloromethane	75-09-2	84.93	1325	Macklin-Shanghai	0.995
acetonitrile	75-05-8	41.05	790	Macklin-Shanghai	0.996
isopropanol	67-63-0	60.06	785.1	Macklin-Shanghai	0.997

[a]Taken from ref 32. [b]*N,N′*-di(1-naphthyl)-*N,N′*-diphenyl benzidine (NPB) was used to verify the reliability of the measurement method for mCP solubility.

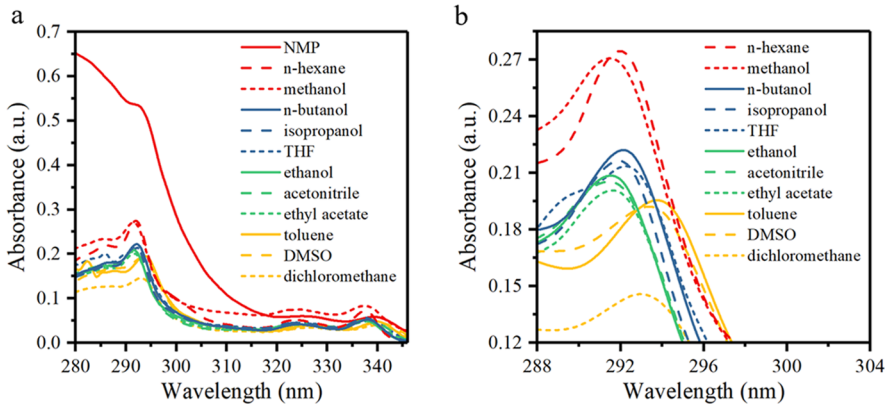

Figure 2. (a) Ultraviolet absorption spectra of mCP from 280 to 346 nm in various solvents: NMP, *n*-hexane, methanol, *n*-butanol, isopropanol, THF, ethanol, acetonitrile, ethyl acetate, toluene, DMSO, and dichloromethane; (b) enlarged view of (a) from 288 to 304 nm in the aforementioned solvents except NMP. The concentration of mCP was 0.002 mg mL^{-1} uniformly when the spectra of all solvents were measured.

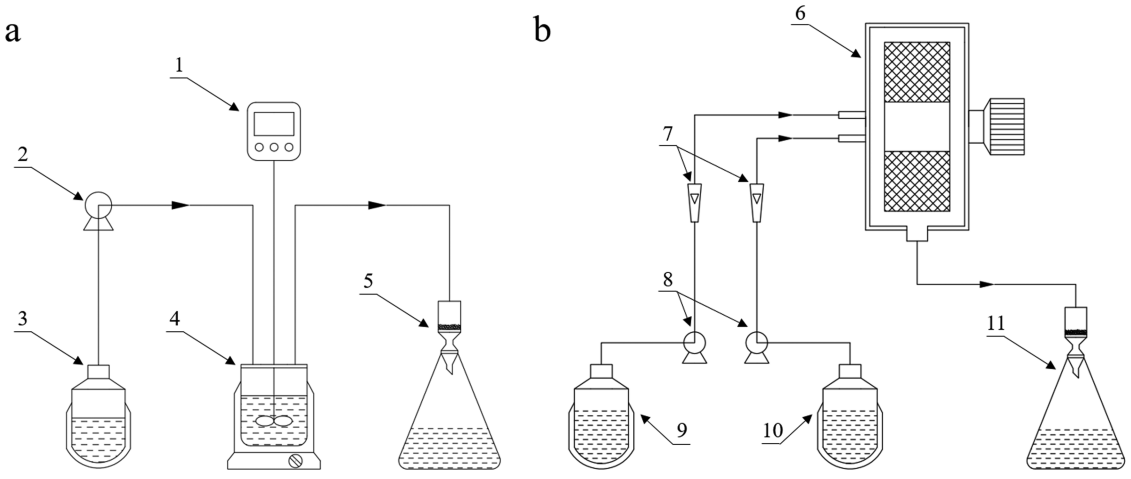

Figure 3. Experimental device diagrams of (a) stirred-tank reactor and (b) rotating packed-bed reactor. (1, digital display mixer; 2 and 8, pumps; 3 and 9, SP storage containers; 4, constant temperature stirred-tank reactor with ASP; 5 and 11, vacuum filters; 6, rotating packed-bed reactor; 7, flow meters; and 10, ASP storage container).

283.15 to 313.15 K for common experimental operations in practical applications, minimally affecting the material composition. The modified Apelblat equation was applied to correlate the experimental solubility data of mCP. The precipitation of mCP via the SAS method in both the conversional stirred-tank reactor (STR) and rotating packed bed (RPB) was devised. The morphology changes in the precipitated mCP products under different experimental conditions were preliminarily studied,

DOI: 10.1021/acs.jced.9b00432
J. Chem. Eng. Data 2019, 64, 4349−4356

Table 2. Calibration Equations of 1,3-Bis(9-carbazolyl)benzene (mCP) in Organic Solvents[a]

solvents	λ_{max} (nm)	calibration equation	R^2	s
methanol	293	Abs = 68.4 × Con + 0.029	0.9999	0.0027
isopropanol	292	Abs = 111.2 × Con − 0.0006	0.9999	0.0025
n-butanol	292	Abs = 122.5 × Con − 0.013	0.9996	0.0070
n-hexane	292	Abs = 137.6 × Con − 0.004	0.9990	0.0094
acetonitrile	291	Abs = 58.2 × Con + 0.034	0.9991	0.0026
ethanol	292	Abs = 102.1 × Con + 0.004	0.9999	0.0055
DMSO	293	Abs = 92.8 × Con + 0.009	0.9997	0.0062
ethyl acetate	292	Abs = 105.8 × Con − 0.008	0.9993	0.0063
toluene	294	Abs = 100.7 × Con − 0.005	0.9995	0.0034
THF	292	Abs = 107.8 × Con − 0.0003	0.9994	0.0095
NMP	339[b]	Abs = 28.0 × Con + 0.006	0.9986	0.0029
dichloromethane	292	Abs = 105.4 × Con − 0.006	0.9999	0.0052

[a]λ_{max}: the peak wavelengths of the absorption spectra of mCP in the solvents, R^2: the coefficient of determination, s: the regression standard deviation of the calibration equations. [b]The second peak in 339 nm was chosen because there was a strong background absorption of around 292 nm in NMP.

Table 3. Experimental Results of *N,N′*-Di(1-naphthyl)-*N,N′*-diphenyl Benzidine (NPB) in Two Organic Solvents at Temperature T = 298.15 K and Pressure p = 0.1 MPa[a]

solvents	λ_{max} (nm)	calibration equation	R^2	s	x	100RE
toluene	341	Abs = 66.35 × Con + 0.0023	0.9999	0.0022	5.6×10^{-4}	−3.62
NMP[b]	342	Abs = 55.34 × Con + 0.0047	0.9999	0.0013	2.3×10^{-3}	−0.87

[a]λ_{max}: the peak wavelengths of the absorption spectra of NPB in the solvents, R^2: the coefficient of determination, s: the regression standard deviation of the calibration equations, x: the experimental mole fraction solubility of NPB, RE: the relative error between the experimental solubility data in our work and the reported data in ref 18. Standard uncertainties u are $u(T)$ = 0.05 K, $u(p)$ = 0.02 MPa. The relative standard uncertainty of the solubility u_r is $u_r(x)$ = 0.04. [b]NMP: 1-methyl-2-pyrrolidinone.

which laid a foundation for the preparation of the nanodispersion of mCP for OLED devices via solution processing.

2. EXPERIMENTAL SECTION

2.1. Materials. mCP (mass fraction purity ≥ 97.0%) was purchased from Sigma-Aldrich. The information for materials and solvents is shown in Table 1. All chemical materials were used as received without further purification.

2.2. Solubility Measurement. The solubility of mCP in various organic solvents was determined by the isothermal saturation method, which is the solubility of the saturated solution, and was measured by an ultraviolet−visible (UV) spectrometer after isothermal dilution. Briefly, an excessive amount of mCP was mixed with the solvent into a small glass tube. For a specific amount of mCP and the solvent, accuracy was not needed if the mixture gave a saturated solution. The mixture was sonicated for 30 min in an ultrasonic cleaner (KQ2200B, Jiangsu Kunshan Ultrasonic Instrument Co.) and the temperature was guaranteed to exceed the target temperature point. After cooling the mixture to the target measuring temperature in a constant temperature water bath and maintaining the mixture for 2 h, the excess solid phase was observed. The mixture was filtered through a PTFE membrane filter (0.2 μm pore size) to obtain the saturated solution of mCP. Then, the saturated solution was diluted with the proportional organic solvent at room temperature (298.15 K). The diluted solution was loaded into a quartz cuvette with an optical path length b = 1 cm. The final absorbance was measured by a UV spectrophotometer (Shimadzu UV-2600). The experiments were repeated five times at each temperature point to ensure the accuracy of the results. The absorption spectra of mCP in various solvents at a fixed concentration (0.002 mg mL^{-1}) are shown in Figure 2.

The UV absorption peak wavelength of mCP is in the range of 290−295 nm. As shown in Figure 2, the wavelength values (λ_{max}) corresponding to the absorption peaks in different solvents varied slightly because of the dispersion interaction with organic solvents. In particular, due to the strong absorption of NMP near 292 nm, the second absorption peak (around 339 nm) was selected as the measurement point.[33] Therefore, we used the peak absorbance A_{max} corresponding to the peak wavelength to calculate the concentration of mCP in the solution, instead of the fixed wavelength. According to the Lambert−Beer law[34]

$$C = \frac{A_{max}}{\varepsilon b} \quad (1)$$

where C is the molarity concentration of the drugs and ε is the molar absorption coefficient of mCP. There is an explanation that the absorbance A_{max} of the diluted solution needs to be less than or equal to 1.2 to satisfy the Lambert−Beer law.

2.3. Preparation of Antisolvent Precipitation. The antisolvent precipitation experiment of mCP was mainly divided into two types: the first one was conventional mixing in conversional STR and the other was rotating packed-bed reactor (RPB) strengthening. The schematic diagram of the facilities is shown in Figure 3. The fundamental principle of RPB strengthening is to optimize the mass transfer process between solvents and antisolvents by centrifugal force in RPB.[34−36]

In brief, mCP was dissolved in NMP with high solubility to form the solvent phase (SP). The antisolvent phase (ASP) mainly consisted of deionized water. To study the influence of different conditions on the precipitation results, the components of ASP also included water + methanol or water + surfactant. In the STR route (Figure 3a), ASP was placed in a constant temperature water bath (4) and stirred at a set speed by the

DOI: 10.1021/acs.jced.9b00432
J. Chem. Eng. Data 2019, 64, 4349−4356

Table 4. Experimental Mole Fraction Solubility x of 1,3-Bis(9-carbazolyl)benzene (mCP) in Various Organic Solvents at Temperature T (K) and Pressure p = 0.1 MPa[a]

solvent	T (K)	10^3x	solvent	T (K)	10^3x	solvent	T (K)	10^3x
methanol	283.15	0.0436	isopropanol	283.15	0.0455	*n*-butanol	283.15	0.122
	293.15	0.0614		293.15	0.0590		293.15	0.170
	303.15	0.0966		303.15	0.0695		303.15	0.217
	313.15	0.108		313.15	0.110		313.15	0.318
n-hexane	283.15	0.183	acetonitrile	283.15	0.243	ethanol	283.15	0.448
	293.15	0.259		293.15	0.311		293.15	0.561
	303.15	0.342		303.15	0.363		303.15	0.802
	313.15	0.381		313.15	0.483		313.15	1.09
DMSO	293.15	4.36	ethyl acetate	283.15	4.26	toluene	283.15	26.3
	303.15	4.43		293.15	5.99		293.15	31.6
	313.15	4.72		303.15	8.27		303.15	33.6
	323.15	5.05		313.15	8.79		313.15	44.5
THF	283.15	50.7	NMP	283.15	62.0	dichloromethane	273.15	94.9
	293.15	52.8		293.15	70.2		283.15	107
	303.15	59.8		303.15	76.1		293.15	112
	313.15	79.2		313.15	80.1		303.15	139

[a]Standard uncertainties for temperature and pressure are $u(T)$ = 0.05 K and $u(p)$ = 0.02 MPa. Relative standard uncertainty for solubility is $u_r(x)$ = 0.13.

digital display mixer (1). According to the calculated volume, SP was quickly added to the ASP at the same temperature (293.15 K). During this process, the mixture rapidly nucleated and produced particles due to the sudden increase in supersaturation.[37] After stirring for 5 min, the suspension was vacuum-pumped and filtered by a PTFE membrane filter with a 0.2 μm pore size (5). In the RPB route (Figure 3b), the SP and the ASP were transferred into the rotating packed bed (6) by pumps (8) according to the fixed volume ratio. The two phases were immediately mixed by liquid distributors in the filling of the rotor at a temperature of 293.15 K. Then, the suspension was collected from the outlet and vacuum-pumped simultaneously (11). Finally, the filtered residue obtained from the two experimental modes was collected and vacuum-dried for further characterization and testing.

2.4. Characterization. The UV absorption spectra were characterized by a Shimadzu UV-2600 spectrophotometer. For antisolvent precipitation experiments, the morphology studies were performed using a JEOL JSM-7800F scanning electron microscope (SEM). The Fourier transform infrared (FTIR) spectra of experimental products and raw materials were measured by a Bruker Vector-70v FTIR spectrometer.

2.5. Calculation of the Solubility. All solubility data at each temperature point were calculated using a calibration equation, which was determined by the proportional relationship between absorbance and concentration. Every calibration equation in the form of eq 2 was plotted with absorbance data at a series of exact concentration points

$$\mathrm{Abs} = A \times \mathrm{Con} + B \tag{2}$$

where A and B are the slope and the intercept in the proportional relationship, respectively. Con means the concentration of mCP (mg mL^{-1}) and Abs is the absorbance. The specific peak wavelengths and calibration equations corresponding to the 12 organic solvents are shown in Table 2.

The solubility of investigated solutes was calculated using 3

$$x^{\mathrm{e}} = \frac{m_1/M_1}{m_1/M_1 + m_2/M_2} \tag{3}$$

where x^{e} is the mole fraction solubility of the solute, m_1 and m_2 are the respective mass (g) of the solute (mCP) and the corresponding solvent, and M_1 and M_2 represent the molar mass (g moL^{-1}) of the solute and the solvent, respectively.

2.6. Verification of the Measurement Methods. Currently, the solubility data of mCP have not been reported. To prove the validity and reliability of the measurement method used in this article, we measured the solubility of *N,N′*-di(1-naphthyl)-*N,N′*-diphenyl benzidine (NPB), a typical hole-transport material of OLED devices, in the same way in two organic solvents. Specifically, we chose toluene and NMP with large solubility differences reported in the literature.[18] The measuring conditions of the experiment were T = 298.15 K and p = 0.1 MPa, the same as those given in the literature.[18] The results are listed in Table 3, which shows that the experimental data are basically consistent with the literature results. Hence, the measurement method can be used to determine the solubility of mCP.

3. RESULTS AND DISCUSSION

3.1. Solubility. Table 4 shows the experimental solubility data of mCP in methanol, isopropanol, *n*-butanol, *n*-hexane, acetonitrile, ethanol, DMSO, ethyl acetate, toluene, THF, NMP, and dichloromethane in the main temperature range from 283.15 to 313.15 K. Especially, the melting point of DMSO and the boiling point of dichloromethane are included in the main temperature range, which could influence the measuring conditions, so their temperature ranges were adjusted from 293.15 to 323.15 K and 273.15 to 303.15 K, respectively.

3.2. Solubility Modeling. Figure 4 shows the plots of ln x versus the inverse of temperature (K^{-1}), where x represents the mole fraction solubility of mCP and T is the measured temperature of each solvent. Table 4 also indicates that the solubility decreases based on the following order in different solvents: dichloromethane > NMP > THF > toluene > ethyl acetate > DMSO > ethanol > acetonitrile > *n*-hexane > *n*-butanol > (methanol, isopropanol). Correspondingly, Figure 4 summarizes the 12 solvents. The experimental results indicate that the solubility of all solutes is strongly dependent on the temperature of the solvent, and the solubility increases with increasing

DOI: 10.1021/acs.jced.9b00432
J. Chem. Eng. Data 2019, 64, 4349−4356

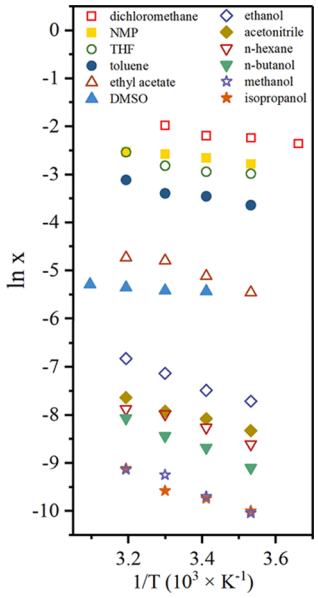

Figure 4. Plots of ln x versus the inverse of temperature (K^{-1}). x represents the mole fraction solubility of mCP in various solvents: □, dichloromethane; ■, NMP; ○, THF; ●, toluene; △, ethyl acetate; ▲, DMSO; ◇, ethanol; ◆, acetonitrile; ▽, *n*-hexane; ▼, *n*-butanol; ☆, methanol; ★, isopropanol.

Table 5. Solubility Parameters of 1,3-Bis(9-carbazolyl)benzene (mCP) in Organic Solvents from Modified Apelblat Equation

solvent	*A*	*B*	*C*	$10^3 \times$ RMSD[a]
methanol	145.55	−9137.69	−21.84	0.01
isopropanol	−112.37	2257.81	16.71	0.01
n-butanol	−120.42	2546.70	18.14	0.01
n-hexane	187.97	−10489.81	−28.25	0.01
acetonitrile	−96.82	2238.58	14.27	0.01
ethanol	−97.91	1691.58	14.91	0.02
DMSO	−100.44	3940.07	14.36	0.04
ethyl acetate	126.72	−7593.07	−18.65	0.44
toluene	−103.16	3153.01	15.65	1.59
THF	−106.93	3435.95	16.25	3.44
NMP	178.25	−8680.46	−26.63	0.10
dichloromethane	−328.29	13237.58	49.46	3.19

[a]RMSD is the root-mean-square deviation between the calculated and experimental solubility.

temperature. The solubility dependence of mCP in 12 pure solvents was correlated using the modified Apelblat equation.[4][38−40]

$$\ln x = A + \frac{B}{T/K} + C \ln(T/K) \tag{4}$$

where x is the mole fraction solubility of mCP in 12 organic solvents; T is the absolute temperature; and A, B, and C refer to empirical parameters.

Besides, the root-mean-square deviation (RMSD) was calculated using the following equation[5]

$$\mathrm{RMSD} = \sqrt{\frac{1}{N}\sum_{i=1}^{N}(x^{c} - x^{e})^{2}} \tag{5}$$

where N represents the number of experimental data points, and x^c and x^e refer to the calculated and experimental mole fraction solubility of mCP, respectively.

Table 5 lists the empirical parameters' values of A, B, and C for every solvent and the respective RMSD. The experimental solubility data and the predicted solubility data for eq 4 are shown in Figure 5. It can be seen that the modified Apelblat equation agrees well with the experimental data for the solubility of the selected solvents in their respective temperature range. It should be noted that the mass purity of mCP used in the experiment is 97%. The impurities may have a strong impact on the solubility of mCP in the solvent. Our findings based on the experimental measurements for the solubility of mCP in 12 kinds of organic solvents at atmospheric pressure in the temperature range of 283.15−313.15 K suggest that the increase of temperature would lead to the increase of mCP solubility, and the correlated values based on the modified Apelblat equation agreed well with the experimental values. The knowledge obtained offered fundamental guidelines for the future design of mCP nanodispersion via solution processing.

3.3. Solvent−Antisolvent Precipitation of mCP. The experimental conditions and main results for the antisolvent precipitation experiments are summarized in Table 6. The stabilities of mCP in the six experiments were analyzed by the FTIR spectra. Figure 6 shows the FTIR spectra of the raw material and five products obtained from antisolvent precipitation experiments. There was no significant difference between the raw material and the products in the selected samples. The fingerprint patterns of FTIR before and after the antisolvent precipitation process were basically consistent, indicating that the composition of mCP did not change in the experiment.

The morphology of raw materials and antisolvent precipitation samples was observed under SEM, as shown in Figure 7. To avoid recrystallization caused by dissolution of organic solvents, SEM images of all samples were dispersed with water. Obviously, outcomes with different shapes and sizes were produced under different experimental conditions. In RPB experiments 1 and 2, the basic morphology of the products was clavate crystal (Figure 7a,b). The only difference between the two RPB experiments was the rotor speed. The higher rotational speed in experiment 2 resulted in finer crystals. In contrast, the products from STR experiments were generally polyhedral or spherical particles. The product morphology obtained in STR experiments 3, 4, and 5 corresponds to Figure 7d, e, and f, respectively. Compared with experiment 3, ASP in STR experiment 5 was the mixture of methanol and water, which led to tiny spheres of about 30 nm in diameter (Figure 7f). The effect of surfactants (PVP) on nucleation was also studied. The addition of PVP caused the particles to change from ellipsoids to clumps, and the size was reduced by half. In the absence of a surfactant coating, the cooling of the suspension during the vacuum filtration process may result in larger product sizes. Further controlled preparation of the appearance of antisolvent precipitation outcomes is under study. Optimizing conditions under study include SP and ASP volume ratio change, concentration adjustment, and so on.

4. CONCLUSIONS

In this work, the solubility of mCP was measured in 12 organic solvents of methanol, ethanol, isopropanol, *n*-butanol, ethyl acetate, *n*-hexane, dichloromethane, toluene, acetonitrile, THF, NMP, and DMSO in the major temperature range from 283.15 to 313.15 K at atmospheric pressure. The results show that the

DOI: 10.1021/acs.jced.9b00432
J. Chem. Eng. Data 2019, 64, 4349−4356

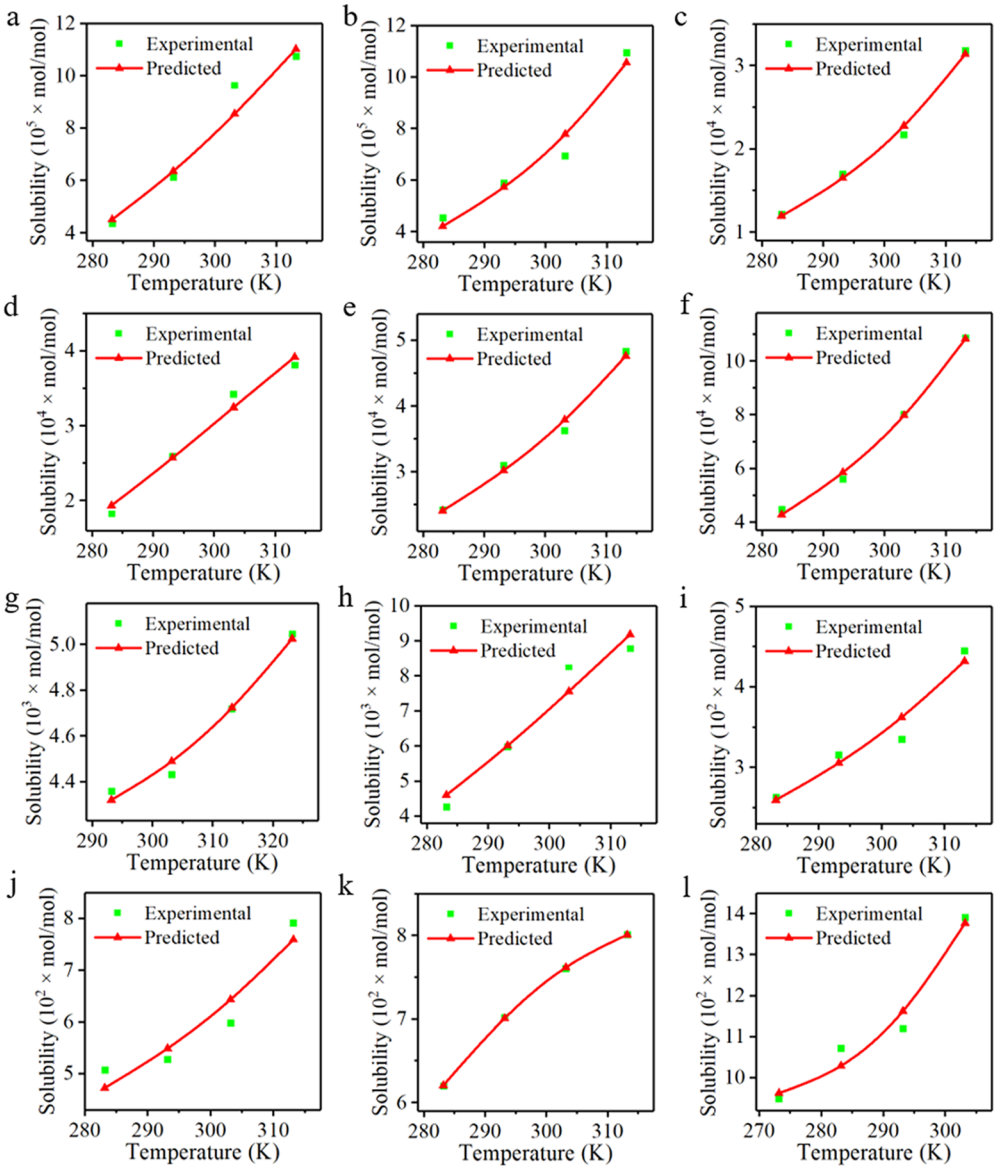

Figure 5. Experimental and predicted mole fraction solubility of methanol (a), isopropanol (b), *n*-butanol (c), *n*-hexane (d), acetonitrile (e), ethanol (f), DMSO (g), ethyl acetate (h), toluene (i), THF (j), NMP (k), and dichloromethane (l) as a function of temperature.

Table 6. Antisolvent Precipitation Experimental Conditions and Results Summary

	experimental conditions						results	
exp.	reactor	antisolvent	volume ratio (SP:ASP)	concentration (mol g^{-1})	surfactant	rotor speed (r min^{-1})	max. length[a] (SEM)	morphology
1	RPB	water	1:10	9.5		2240	3.2 ± 0.1 μm	thick clavate crystals
2	RPB	water	1:10	9.5		2540	2.0 ± 0.1 μm	fine virgate crystals
3	STR	water	1:10	23.8		600	1.0 ± 0.1 μm	stacked ellipsoids
4	STR	water	1:10	23.8	PVP[b]	600	500.0 ± 200.0 nm	varisized clumps
5	STR	MeOH + water	1:(2 + 10)	23.8		600	33.0 ± 0.7 nm	tiny spheres

[a]Observed from the scanning electron microscope (SEM) images. [b]PVP, poly(vinylpyrrolidone).

solubility of mCP in each solvent increases with the increase of temperature. The solubility data in all solvents can be correlated well by the modified Apelblat equation. The maximum value of RMSD between the measured solubility and the predicted solubility was 3.44×10^{-3}. The antisolvent precipitation experiments of mCP under different conditions were preliminarily studied. It can be concluded from the experiment that different experimental conditions could effectively control the product morphology and size. Specifically, the product obtained by the RPB mode was a rod-shaped crystal. The higher the rotor speed, the finer the clavate crystal. The results of STR patterns were spherical or irregular particles. The particle size obtained when ASP was methanol and water was 1/30th of that obtained when ASP was only water. When PVP as a stabilizer was added into ASP, the particles became smaller and the morphology changed from elliptic to lumpish. Our preliminary study

DOI: 10.1021/acs.jced.9b00432
J. Chem. Eng. Data 2019, 64, 4349−4356

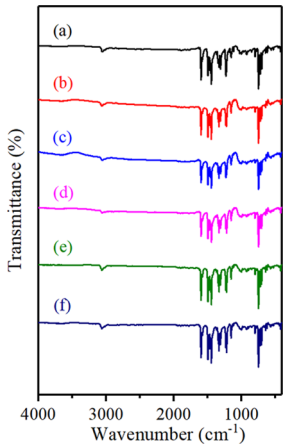

Figure 6. FTIR spectra of (a) raw materials of mCP and (b–f) precipitation products from experiments 1–5, respectively. The major characteristics of products (b–f), corresponding to experiments 1–5, are as follows: (b) in RPB at 2240 r min^{-1}; (c) in RPB at 2540 r min^{-1}; (d) in STR at 600 r min^{-1}; (e) in STR at 600 r min^{-1}, with surfactant poly(vinylpyrrolidone) (PVP); (f) in STR at 600 r min^{-1}, with a different antisolvent phase MeOH and water.

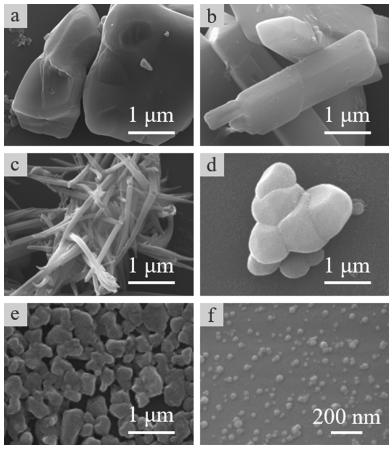

Figure 7. SEM images of (a) raw mCP and precipitation products at experimental conditions (b) 1, (c) 2, (d) 3, (e) 4, and (f) 5, respectively.

illustrated that nanonization of poorly soluble organic materials is promising for the preparation of inks of OLED materials for solution processing and related work in the future.

AUTHOR INFORMATION

Corresponding Author

*E-mail: wangdan@mail.buct.edu.cn. Tel: +86 10 64449453.

ORCID

Jie-Xin Wang: 0000-0003-0459-1621

Dan Wang: 0000-0002-3515-4590

Notes

The authors declare no competing financial interest.

ACKNOWLEDGMENTS

The authors are grateful for financial support from the National Key Research and Development Program of China (2017YFB0404400).

REFERENCES

(1) Reineke, S.; Lindner, F.; Schwartz, G.; Seidler, N.; Walzer, K.; Lüssem, B.; Leo, K. White Organic Light-Emitting Diodes with Fluorescent Tube Efficiency. *Nature* **2009**, *459*, 234–238.

(2) Park, J. S.; Kim, T. W.; Stryakhilev, D.; Lee, J. S.; An, S. G.; Pyo, Y. S.; Lee, D. B.; Mo, Y. G.; Jin, D. U.; Chung, H. K. Flexible Full Color Organic Light-Emitting Diode Display on Polyimide Plastic Substrate Driven by Amorphous Indium Gallium Zinc Oxide Thin-Film Transistors. *Appl. Phys. Lett.* **2009**, *95*, No. 013503.

(3) Lee, S. Y.; Yasuda, T.; Nomura, H.; Adachi, C. High-Efficiency Organic Light-Emitting Diodes Utilizing Thermally Activated Delayed Fluorescence from Triazine-Based Donor-Acceptor Hybrid Molecules. *Appl. Phys. Lett.* **2012**, *101*, No. 093306.

(4) Chen, H. W.; Lee, J. H.; Lin, B. Y.; Chen, S.; Wu, S. T. Liquid Crystal Display and Organic Light-Emitting Diode Display: Present Status and Future Perspectives. *Light: Sci. Appl.* **2018**, *7*, No. 17168.

(5) Choi, M. K.; Yang, J.; Hyeon, T.; Kim, D. H. Flexible Quantum Dot Light-Emitting Diodes for Next-Generation Displays. *NPJ Flexible Electron.* **2018**, *2*, No. 10.

(6) Pardo, D. A.; Jabbour, G. E.; Peyghambarian, N. Application of Screen Printing in the Fabrication of Organic Light-Emitting Devices. *Adv. Mater.* **2010**, *12*, 1249–1252.

(7) van der Vaart, N. C.; Lifka, H.; Budzelaar, F. P. M.; Rubingh, J. E. J. M.; Hoppenbrouwers, J. J. L.; Dijksman, J. F.; Verbeek, R. G. F. A.; Van Woudenberg, R.; Vossen, F. J.; Hiddink, M. G. H.; Rosink, J. J. W. M.; Bernards, T. N. M.; Giraldo, A.; Young, N. D.; Fish, D. A.; Childs, M. J.; Steer, W. A.; Lee, D.; George, D. S. Towards Large-Area Full-Color Active-Matrix Printed Polymer OLED Television. *J. Soc. Inf. Disp.* **2005**, *13*, 9–16.

(8) Zhou, L.; Yang, L.; Yu, M. J.; Jiang, Y.; Liu, C. F.; Lai, W. Y.; Huang, W. Inkjet-Printed Small-Molecule Organic Light-Emitting Diodes: Halogen-Free Inks, Printing Optimization, and Large-Area Patterning. *ACS Appl. Mater. Interfaces* **2017**, *9*, 40533–40540.

(9) Yimsiri, P.; Mackley, M. R. Spin and Dip Coating of Light-Emitting Polymer Solutions: Matching Experiment with Modelling. *Chem. Eng. Sci.* **2006**, *61*, 3496–3505.

(10) Li, J.; Xu, L. S.; Tang, C. W.; Shestopalov, A. A. High-Resolution Organic Light Emitting Diodes Patterned via Contact Printing. *ACS Appl. Mater. Interfaces* **2016**, *8*, 16809–16815.

(11) Zysman-Colman, E.; Ghosh, S. S.; Xie, G.; Varghese, S.; Chowdhury, M.; Sharma, N.; Cordes, D. B.; Slawin, A. M. Z.; Samuel, I. D. W. Solution-Processable Silicon Phthalocyanines in Electroluminescent and Photovoltaic Devices. *ACS Appl. Mater. Interfaces* **2016**, *8*, 9247–9253.

(12) Guo, F.; Karl, A.; Xue, Q. F.; Tam, K. C.; Forberich, K.; Brabec, C. J. The Fabrication of Color-Tunable Organic Light-Emitting Diode Displays via Solution Processing. *Light: Sci. Appl.* **2017**, *6*, No. e17094.

(13) Singh, M.; Jou, J. H.; Sahoo, S.; Sujith, S. S.; He, Z. K.; Krucaite, G.; Grigalevicius, S.; Wang, C. W. High Light-Quality OLEDs with a Wet-Processed Single Emissive Layer. *Sci. Rep.* **2018**, *8*, No. 7133.

(14) Villani, F.; Vacca, P.; Nenna, G.; Valentino, O.; Burrasca, G.; Fasolino, T.; Minarini, C.; Sala, D. D. Inkjet Printed Polymer Layer on Flexible Substrate for OLED Applications. *J. Phys. Chem. C* **2009**, *113*, 13398–13402.

(15) Zhong, C. M.; Duan, C. H.; Huang, F.; Wu, H. B.; Cao, Y. Materials and Devices Toward Fully Solution Processable Organic Light-Emitting Diodes. *Chem. Mater.* **2011**, *23*, 326–340.

(16) Ohisa, S.; Pu, Y. J.; Yamada, N. L.; Matsuba, G.; Kido, J. J. Molecular Interdiffusion between Stacked Layers by Solution and Thermal Annealing Processes in Organic Light Emitting Devices. *ACS Appl. Mater. Interfaces* **2015**, *7*, 20779–20785.

(17) Mcewan, J. A.; Clulow, A. J.; Nelson, A.; Vuuren, R. D. J. V.; Burn, P. L.; Gentle, I. R. Morphology of OLED Film Stacks Containing Solution-Processed Phosphorescent Dendrimers. *ACS Appl. Mater. Interfaces* **2018**, *10*, 3848–3855.

(18) Takebayashi, Y.; Morii, N.; Sue, K.; Furuya, T.; Yoda, S.; Ikemizu, D.; Taka, H. Solubility of *N,N′* -Di(1-naphthyl)-*N,N′* -diphenyl Benzidine (NPB) in Various Organic Solvents: Measurement and

DOI: 10.1021/acs.jced.9b00432
J. Chem. Eng. Data 2019, 64, 4349–4356

Correlation with the Hansen Solubility Parameter. *Ind. Eng. Chem. Res.* **2015**, *54*, 8801−8808.
(19) Stolz, S.; Scherer, M.; Mankel, E.; Lovrinčić, R.; Schinke, J.; Kowalsky, W.; Jaegermann, W.; Lemmer, U.; Mechau, N.; Hernandez-Sosa, G. Investigation of Solution-Processed Ultrathin Electron Injection Layers for Organic Light-Emitting Diodes. *ACS Appl. Mater. Interfaces* **2014**, *6*, 6616−6622.
(20) Pu, Y.; Wang, J.-X.; Wang, D.; Foster, N. R.; Chen, J.-F. Subcritical Water Processing for Nanopharmaceuticals. *Chem. Eng. Process.* **2019**, *140*, 36−42.
(21) Pu, Y.; Leng, J.; Wang, D.; Wang, J.-X.; Foster, N. R.; Chen, J.-F. Recent Progress in the Green Synthesis of Rare-earth Doped Upconversion Nanophosphors for Optical Bioimaging from Cells to Animals. *Chin. J. Chem. Eng.* **2018**, *26*, 2206−2218.
(22) Wang, D.; Zhu, L.; Pu, Y.; Wang, J.-X.; Chen, J.-F.; Dai, L. Transferrin-coated Magnetic Upconversion Nanoparticles for Efficient Photodynamic Therapy with Near-infrared Irradiation and Luminescence Bioimaging. *Nanoscale* **2017**, *9*, 11214−11221.
(23) Wang, D.; Wang, Z.; Zhan, Q.; Pu, Y.; Wang, J.-X.; Foster, N. R.; Dai, L. Facile and Scalable Preparation of Fluorescent Carbon Dots for Multifunctional Applications. *Engineering* **2017**, *3*, 402−408.
(24) Gao, Z.; Rohani, S.; Gong, J.; Wang, J. Recent Developments in the Crystallization Process: Toward the Pharmaceutical Industry. *Engineering* **2017**, *3*, 343−353.
(25) Pu, Y.; Wen, X.; Li, Y.; Wang, D.; Foster, N. R.; Chen, J.-F. Ultrafine Clarithromycin Nanoparticles via Anti-solvent Precipitation in Subcritical Water: Effect of Operating Parameters. *Powder Technol.* **2017**, *305*, 125−131.
(26) Pu, Y.; Li, Y.; Wang, D.; Foster, N. R.; Wang, J.-X.; Chen, J.-F. A Green Route to Beclomethasone Dipropionate Nanoparticles via Solvent Anti-solvent Precipitation by Using Subcritical Water as the Solvent. *Powder Technol.* **2017**, *308*, 200−205.
(27) Wang, X. D.; Wang, S. M.; Ma, Z. H.; Ding, J. Q.; Wang, L. X.; Jing, X. B.; Wang, F. S. Solution-Processible 2,2′-Dimethyl-biphenyl Cored Carbazole Dendrimers as Universal Hosts for Efficient Blue, Green, and Red Phosphorescent OLEDs. *Adv. Funct. Mater.* **2014**, *24*, 3413−3421.
(28) Sun, D. M.; Zhou, X. K.; Liu, J. T.; Sun, X. L.; Li, H. H.; Ren, Z. J.; Ma, D. G.; Bryce, M. R.; Yan, S. K. Solution-Processed Blue/Deep Blue and White Phosphorescent Organic Light-Emitting Diodes (PhOLEDs) Hosted by a Polysiloxane Derivative with Pendant mCP (1,3-bis(9-carbazolyl)benzene). *ACS Appl. Mater. Interfaces* **2015**, *7*, 27989−27998.
(29) Wang, J.; Liu, J.; Huang, S. J.; Wu, X. K.; Shi, X. D.; Chen, C. P.; Ye, Z. C.; Lu, J. G.; Su, Y. K.; He, G. F.; Zheng, Y. X. High Efficiency Green Phosphorescent Organic Light-Emitting Diodes with a Low Roll-Off at High Brightness. *Org. Electron.* **2013**, *14*, 2854−2858.
(30) Kwon, S.; Kim, T. G.; Choi, W. K.; Kang, S. O.; Kim, J. W. Order-Disorder Transition in the Molecular Orientation during Initial Growth of Organic Thin Film. *ACS Appl. Mater. Interfaces* **2013**, *5*, 1896−1901.
(31) Sun, D. M.; Yang, Z. M.; Ren, Z. J.; Li, H. H.; Bryce, M. R.; Ma, D. G.; Yan, S. K. Oligosiloxane Functionalized with Pendant (1,3-Bis(9-carbazolyl)benzene) (mCP) for Solution-Processed Organic Electronics. *Chem. - Eur. J.* **2014**, *20*, 16233−16241.
(32) Xu, R. J.; Xu, A. L.; Du, C. B.; Cong, Y.; Wang, J. Solubility Determination and Thermodynamic Modeling of 2,4-dinitroaniline in Nine Organic Solvents from T = (278.15 to 318.15) K and Mixing Properties of Solutions. *J. Chem. Thermodyn.* **2016**, *102*, 178−187.
(33) Paredes, J. I.; Villar, R. S.; Martínez, A. A.; Tascón, J. M. D. Graphene Oxide Dispersions in Organic Solvents. *Langmuir* **2008**, *24*, 10560−10564.
(34) Wang, Z.; Su, R.; Wang, D.; Shi, J.; Wang, J.-X.; Pu, Y.; Chen, J.-F. Sulfurized Graphene as Efficient Metal-free Catalysts for Reduction of 4-nitrophenol to 4-aminophenol. *Ind. Eng. Chem. Res.* **2017**, *56*, 13610−13617.
(35) Leng, J.; Chen, J.; Wang, D.; Wang, J.-X.; Pu, Y.; Chen, J.-F. Scalable Preparation of Gd_2O_3:Yb^{3+}/Er^{3+} Upconversion Nanophosphors in a High-gravity rotating Packed Bed Reactor for Transparent Upconversion Luminescent Films. *Ind. Eng. Chem. Res.* **2017**, *56*, 7977−7983.
(36) Pu, Y.; Leng, J.; Wang, D.; Wang, J.; Foster, N. R.; Chen, J.-F. Process Intensification for Scalable Synthesis of Ytterbium and Erbium co-doped Sodium Yttrium Fluoride Upconversion Nanodispersions. *Powder Technol.* **2018**, *340*, 208−216.
(37) He, X.; Tang, R.; Pu, Y.; Wang, J.-X.; Wang, Z.; Wang, D.; Chen, J.-F. High-gravity-hydrolysis Approach to Transparent Nanozirconia/silicone Encapsulation Materials of Light Emitting Diodes Devices for Healthy Lighting. *Nano Energy* **2019**, *62*, 1−10.
(38) Nagy, Z. K.; Fujiwara, M.; Braatz, R. D. Modelling and Control of Combined Cooling and Antisolvent Crystallization Processes. *J. Process Control* **2008**, *18*, 856−864.
(39) Zhang, Y. Q.; Guo, F.; Cui, Q.; Lu, M. Y.; Song, X. L.; Tang, H. J.; Li, Q. S. Measurement and Correlation of the Solubility of Vanillic Acid in Eight Pure and Water + Ethanol Mixed Solvents at Temperatures from (293.15 to 323.15) K. *J. Chem. Eng. Data* **2016**, *61*, 420−429.
(40) Pu, Y.; Cai, F. H.; Wang, D.; Li, Y. H.; Chen, X. Y.; Maimouna, A. G.; Wu, Z. X.; Wen, X. F.; Chen, J.-F.; Foster, N. R. Solubility of Bicalutamide, Megestrol Acetate, Prednisolone, Beclomethasone Dipropionate, and Clarithromycin in Subcritical Water at Different Temperatures from 383.15 to 443.15 K. *J. Chem. Eng. Data* **2017**, *62*, 1139−1145.

DOI: 10.1021/acs.jced.9b00432
J. Chem. Eng. Data 2019, 64, 4349−4356